Experimental study of the heat transfer problem in expansion devices in CO_2 refrigeration systems

Mikolaj Mastrowski[a], Jacek Smolka[a,*], Armin Hafner[b], Michal Haida[a], Michal Palacz[a], Krzysztof Banasiak[c]

[a]*Institute of Thermal Technology, Silesian University of Technology, Konarskiego 22, 44-100 Gliwice, Poland*
[b]*NTNU Department of Energy and Process Engineering, Kolbjrn Hejes vei 1d, 7465 Trondheim, Norway*
[c]*SINTEF Energy, Kolbjrn Hejes vei 1d, 7465 Trondheim, Norway*

Abstract

Two expansion devices designed for CO_2 refrigeration systems namely, capillary tube and fixed-geometry ejector were experimentally tested in the SINTEF/NTNU laboratory in Trondheim, Norway to determine the influence of ambient conditions on their performance. The novelty of this research was to examine the influence of heat transfer between the expansion device wall and the ambient on the R744 flow inside. To achieve this goal, both aforementioned expansion devices were tested with thermally insulated and uninsulated walls. A wide range of operating conditions typical for transcritical CO_2 refrigeration systems were examined. The relatively high ambient temperatures, which occurred during experiments, simulated the realistic conditions in the machine-room of the refrigeration system. The capillary tube consisted of sections of the same length and number of bends. Temperature and differential pressure sensors were placed between those sections to investigate the characteristics of CO_2 within the capillary tube. To measure the inner wall temperature using thermocouples, a prototype R744 ejector with drilled channels was prepared. Ambient conditions did not significantly affect the operation of the capillary tube. Similar conclusions were made for the R744 ejector. However, a slight effect on the temperature of the ejector's wall was observed.

Keywords: carbon dioxide, refrigeration system, capillary tube, ejector, experimental study, heat transfer

Nomenclature

Abbreviations

CA - capillary tube with adiabatic walls
CFD - computational fluid dynamics
CNA - capillary tube with non-adiabatic walls
EA - ejector with adiabatic walls
ENA - ejector with non-adiabatic walls
GWP - global warming potential
ODP - ozone depletion potential

Subscripts

amb - ambient
ej - ejector
IN - capillary tube inlet
MID - capillary tube middle
mn - ejector motive nozzle
out - outlet
OUT - capillary tube outlet
sn - ejector suction nozzle
w - wall

Symbols

COP - coefficient of performance, –

*jacek.smolka@polsl.pl

This is the accepted version of an article published in Energy.
DOI: 10.1016/j.energy.2019.02.097

DP - pressure difference, bar

h - specific enthalpy, kJ/kg

M - mass flow rate, kg/min

n - number of measurements

P - absolute pressure, bar

s - specific entropy, kJ/kgK

T - temperature, °C

u - uncertainty of measurement

x- directly measured quantity

y - indirectly measured quantity

Greek symbols

α - reference accuracy

Δ - difference/loss

η - efficiency, –

Φ_m - mass entrainment ratio, –

1. Introduction

According to the Montreal [1] and Kyoto [2] Protocols, refrigerants with high ozone depletion potential (ODP) and global warming potential (GWP) should be gradually phased out from industrial applications. The European Union's F-gas regulation [3] also provides additional restrictions and impediments in the production and use of fluoride gases in EU countries. The EU introduced new responsibilities, limits and sanctions on the producers and users of high GWP working fluids to effectively discourage their further use. As a consequence of these restrictions, natural refrigerants have become the recommended solution in refrigeration industry.

Among natural working fluids, CO_2 is distinguished due to its low flammability and low toxicity. CO_2 is also a by-product of other industrial processes, making it relatively cheap. It is also characterized by high volumetric refrigeration capacity compared to other synthetic or natural refrigerants [4], which is a consequence of higher pressure levels. These properties, among others, led to R744 being reintroduced in the refrigeration and heat pump industry [5]. However, R744 has a high critical pressure and low critical temperature; thus, refrigeration systems, which reject heat to the ambient environment, operates in transcritical mode. Consequently, the discharge temperature and pressure are independent parameters, making it possible to find an optimal discharge pressure level. Heat rejection occurs with a gliding temperature and increased expansion losses appear. These characteristics cause R744s system coefficient of performance (COP) to decrease compared to other refrigerants. Consequently, the COP improvement of R744-based refrigeration/heat pump systems has become an important challenge in refrigeration industry.

However, for small refrigeration units, the high performance of the system is often not the most important issue; compactness, simplicity and low investment cost typically play more important roles. In such systems, simple expansion devices such as the capillary tube are still good options [6, 7]. As a result, it is possible to find many studies of R744 flowing through capillary tubes. However, few experimental results have been published recently. Madsen et al. [8] presented experimental data that showed that properly designed capillary tubes can keep high-side pressure close to the optimum value, yielding a satisfactory COP. Da Silva et al. [9] also reported on an experimental study that showed that a dimensionless correlation can allow for the prediction of the refrigerant mass flow rate based on the inlet pressure, temperature, and geometry of adiabatic capillary tubes. Agrawal et al. [6] also studied adiabatic capillary tubes as expansion devices in a transcritical R744 system and claimed that an optimal refrigerant charge exists in systems with capillary tubes. The experimental investigation of Song et

This is the accepted version of an article published in Energy.
DOI: 10.1016/j.energy.2019.02.097

al. [10] confirmed the promising operation of capillary tubes in a transcritical heat pump system, showing a COP 80% higher than those obtained using an electric expansion valve at various operating conditions. The authors had similar conclusions in [11]. Experimental tests on a heat pump water heater with an adiabatic capillary tube used as an expansion device was also performed by Wang et al. [12]. The results confirmed the importance of capillary length and refrigerant charge. Some experimental tests were also performed for R744 transcritical systems using non-adiabatic capillary tubes (e.g., [13]). However, in that paper, the capillary tube was used as a suction line heat exchanger. In the literature, many theoretical and numerical investigations concerning adiabatic and non-adiabatic R744 capillary tubes are also available [9, 14, 15, 16, 17]. The models predicted experimental data related to capillary tubes with different dimensions and ranges of operating conditions and produced satisfactory results.

Even though many studies of adiabatic and non-adiabatic capillary tubes working in transcritical CO_2 systems have already been published, few comparisons of the two aforementioned configurations exist. To the best knowledge of the authors, the work where the influence of the heat transfer through the wall of the capillary tube on the CO_2 flow inside was examined, was unavailable in the literature. In this study, the heat transfer between a capillary tube and the ambient environment was examined. The experimental procedure and data gathered from the test facility was evaluated based on the literature.

Larger refrigeration systems require modifications to improve their COP to that of systems using synthetic refrigerants. Thus, reducing in expansion losses is a priority for R744 systems. It could be realized, for example, using an ejector. Thanks to its simple design, an ejector effectively increases the performance of the refrigeration system without a high investment cost. An ejector also allows R744 systems to be used in warm climates [18], which has led to the development of R744 transcritical refrigeration and heat pump systems in recent years.

The ejector works as follows: the high-pressure fluid is expanded inside the ejector and increases its velocity in the motive nozzle; the fluid then entrains the low-pressure suction nozzle stream due to differences in pressure and momentum; both fluids then mix, and the pressure increases in the diffuser. In an ejector-based refrigeration system, the refrigerants pressure is lifted at the exit of the evaporator, limiting compressor work.

Despite the simple construction of the ejector, its internal processes are complex due to the high-pressure reduction, phase change, velocity increase of the motive flow, suction flow entrainment, and two-phase mixing that occur within it. Thus, ejectors should be precisely optimized and designed to function properly to provide a large increase in the cycles COP [19]. Many experiments and numerical investigations have improved ejector construction and examined the influence of crucial parameters on its operation.

Lee et al. [20] performed experiments using a variety of ejector geometry parameters (e.g., motive nozzle throat diameter, mixing section length and diameter) and showed that ejector-based air-conditioning system performances were 15% higher than that of conventional configurations. Lucas et al. [21] also presented an experimental study of ejector-based CO_2 systems that achieved an ejector work recovery efficiency of 22%. The experimental investigation performed by Banasiak et al. [22] showed that the ejector used to recover throttling losses in a R744 refrigeration system can improve COP by up to 8% above that of a standard refrigeration system at the same operating conditions. Banasiak et al. [22] demonstrated that the motive nozzle divergence angle affects ejector efficiency

This is the accepted version of an article published in Energy.
DOI: 10.1016/j.energy.2019.02.097

and suggested that a diffuser outlet with a larger diameter tended to increase ejector efficiency. The ejector mixer length and diameter were also shown to require adjustment to specific operating conditions, especially regarding the motive nozzle pressure, to avoid losses due to friction forces and shock wave phenomena. An optimal diffuser angle was also proposed in that study. Minetto et al. [23] experimentally mapped the ejector at different operating conditions and concluded that the maximum pressure lift above 5 bar could be obtained. They also examined oil separation in an ejector-based system. Another experimental study described the optimal mass entrainment ratio of ejectors based on system operating conditions [24].

Palacz et al. [25] optimized the mixing part of the ejector using a numerical model, validated the model with experimental data, and noted that mixer should be long enough to obtain the satisfactory ejector performance. The authors also mentioned that the mixer diameter strongly affects ejector efficiency. This was confirmed by Nakagawa et al. [26], who concluded that inadequate sizing of the mixing section can decrease the COP of the R744 transcritical refrigeration system by up to 10% compared to the optimal case. Liu et al. [27] used experimental data combined with a model to create empirical correlations to determine the isentropic efficiencies of motive and suction nozzle and mixing section of ejector. Crucial dimensions of the ejector were shown to affect those efficiencies. A similar investigation was performed by Zheng et al. [28], who showed the dependencies between motive and suction nozzle isentropic efficiency, and the mixing section and diffuser efficiency as a function of the motive nozzle and mixer areas ratio, the pressure ratio, and the mass entrainment ratio. Bodys et al. [29] numerically compared two R744 ejectors with and without a swirl generator and described the improvement in the mass entrainment ratio when swirl flow occurred at the motive nozzle inlet. Haida et al. [30] mapped the performance of fixed-geometry ejectors working in a multi-ejector module. They used a reduced-order model based on computational fluid dynamics (CFD) and experimental results to describe the area of high ejector efficiency for different operating conditions.

In the aforementioned papers, experimental results were obtained for various ranges of operating conditions, different types of ejectors and various designs. However, in these reports, the influence of ejector thermal insulation was not examined. In the majority of published numerical models, adiabatic ejector walls were assumed. To the best knowledge of the authors, the only paper, where the heat transfer aspect in ejectors were described, was the work of Milazzo et al. [31]. The authors presented CFD results for an R245fa ejector. They claimed that ejector walls should not be considered as adiabatic in order to evaluate correct heat transfer coefficient profile along ejector wall, what can significantly influence the accuracy of numerical simulations. However, this conclusion was not confirmed by any research paper for R744 ejectors. For this reason, such an investigation needs to be performed. Moreover information about the influence of heat transfer on CO_2 ejector operation has a practical meaning, because there is a high increase of R744 refrigeration systems installed. For this reason, high-accuracy numerical model taking into account all physical phenomena should be used to provide optimal ejector performance.

In this study, the effects of wall thermal insulation on the performance of a two-phase flow fixed-geometry ejector operating in a transcritical R744 refrigeration system were investigated. Similar testing was performed using a coiled capillary tube. The typical operating conditions for CO_2 refrigeration systems were considered at the inlets of both expansion devices. The absolute pressure ranged from 64.5 bar to 106.3 bar, and the temperature ranged

This is the accepted version of an article published in Energy.
DOI: 10.1016/j.energy.2019.02.097

from 20.2°C to 33.8°C, which corresponded to a wide range of subcritical and supercritical conditions. Tests were carried out using accurate measuring equipment, including Coriolis-type mass flow metres and piezoelectric pressure sensors. Two variants of the experiment with similar operating conditions were performed for each expansion device to compare the operation with and without thermal insulation. The experimental results obtained from the ejector experiment were further used to validate the CFD model described by Haida et. al [32]. The authors presented the numerical approach, which allowed inner and outer heat transfer analysis in the CO2 ejector. The influence of wall thermal conductivity and roughness, assumed heat transfer coefficient at the ejector outer walls and turbulence intensity of the motive flow on the ejector performance were investigated. Also 4 variants of adiabatic and non-adiabatic inner and outer walls of ejector were considered. It allowed the temperature field and two-phase flow analysis. The CFD results indicated detailed recommendations about ejector construction. It was suggested, that the low-conductivity materials between the motive and suction nozzles should be used to avoid undesirable heat transfer between motive and suction flows. Moreover the axial-type suction nozzle inlet was recommended instead of tangential-type to reduce aforementioned heat transfer influence.

2. Experimental facility and procedure

For this study, a capillary tube and an ejector were examined experimentally at a test facility in the NTNU/SINTEF laboratory in Trondheim, Norway.

2.1. Test facility

The test setup included a one-stage R744 transcritical refrigeration cycle that was adapted to operate with a capillary tube and an ejector. The setup consisted of a primary CO_2 cycle and an auxiliary glycol cycle, as shown in Fig. 1 and 2.

Configuration with a capillary tube

In Fig. 1, the layout of the test setup configured with the capillary tube is shown. The compressor drew vapor in from the liquid separator. The vapor was then superheated in the internal heat exchanger to ensure liquid droplets did not enter the compressor, preventing serious malfunction. Then, the oil was separated from the refrigerant, which was piped to the gas cooler to be cooled with a glycol-water solution. A portion of the flow from the gas cooler flowed to the internal heat exchanger to increase the temperature of the gas at the suction of the compressor. The vapor was then expanded in the capillary tube to the evaporation pressure. Next, the two-phase fluid evaporated, absorbing the heat in the glycol evaporator, and then returned to the liquid separator. The liquid separator has two outlets; the one at the top was used to supply the compressor with CO_2 vapor. Because the oil separator did not completely remove the lubricant after the compressor, a portion of it accumulated at the bottom of the liquid separator. Thus, a second outlet was placed at that location that consisted of a pipe with small diameter to return the oil to the compressor using the suction line. The metering valve on the oil return line was used to control the amount of lubricant returning with the refrigerant to provide proper lubrication to the compressor and prevent high oil levels at the bottom of the liquid separator.

This is the accepted version of an article published in Energy.
DOI: 10.1016/j.energy.2019.02.097

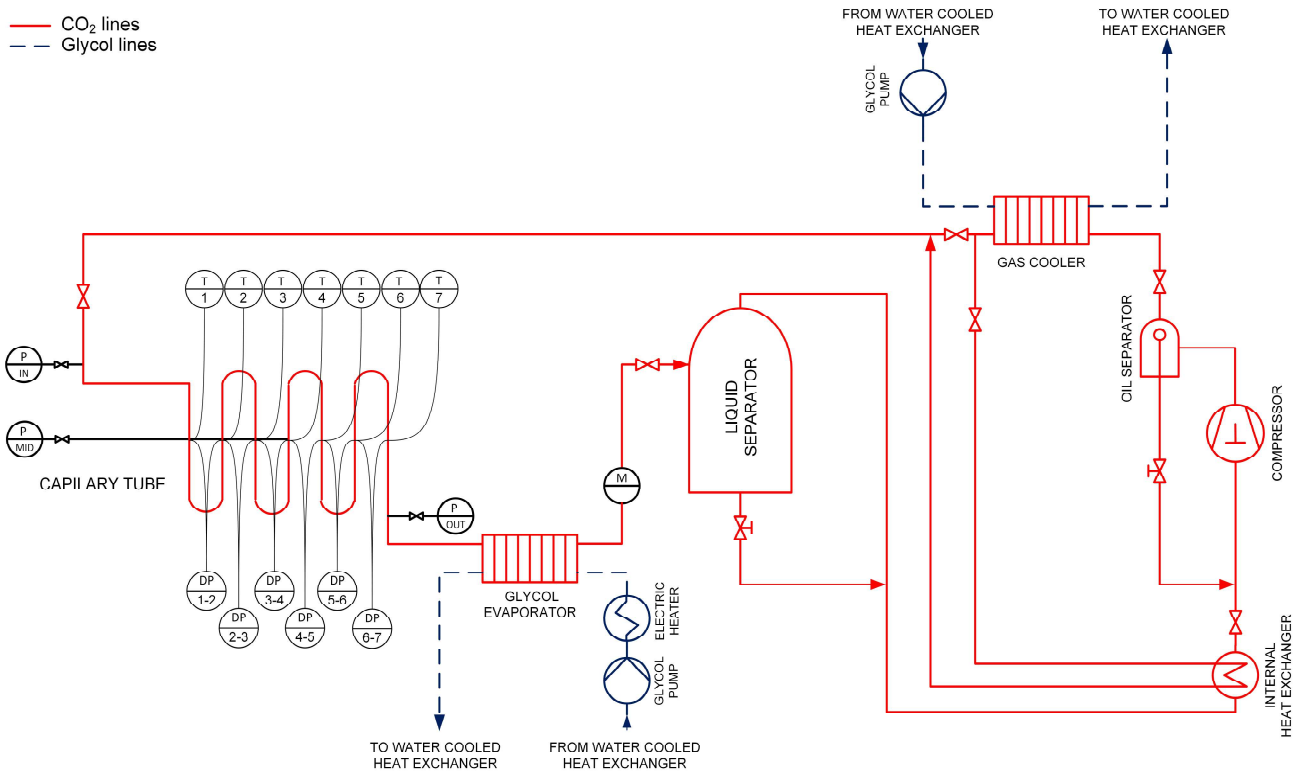

Figure 1: Scheme of the test rig with capillary tube as an expansion device.

The gas cooler capacity was controlled by adjusting the power of the glycol pump, while the evaporator capacity was regulated by adjusting the power of the glycol pump or by heating the glycol with an electric heater in the glycol loop, which supplies the evaporator. It was also possible to change the temperature of the glycol entering the evaporator using a P&ID controller that adjusted the power of the electric heater. Additionally, the compressors rotational speed could be controlled by regulating the transducer connected to the electric motor.

Configuration with ejector

Fig. 2 shows the configuration of the test facility with the ejector installed. The difference from the previous mode occurs after the gas cooler, where the refrigerant expands in the motive nozzle of the ejector. Next, vapor from the evaporator moved via the resulting pressure difference. Pressure was then increased to the separator pressure in the ejector mixer and diffuser, moving the fluid to the liquid separator. The CO_2 liquid from the separator was expanded in the regulated expansion valve and evaporated in the evaporator.

Equipment

The test facility was equipped with the devices specified in Tab. 1. The primary part of the CO_2 cycle was the piston-type compressor, which had a displacement volume of 3 m^3/h and a maximum discharge pressure of 150 bar. An oil separator was installed after the compressor to separate the lubricant from the refrigerant. Brazed-plate CO_2-glycol heat exchangers were used as gas cooler and an evaporator. The liquid separator was designed with

This is the accepted version of an article published in Energy.
DOI: 10.1016/j.energy.2019.02.097

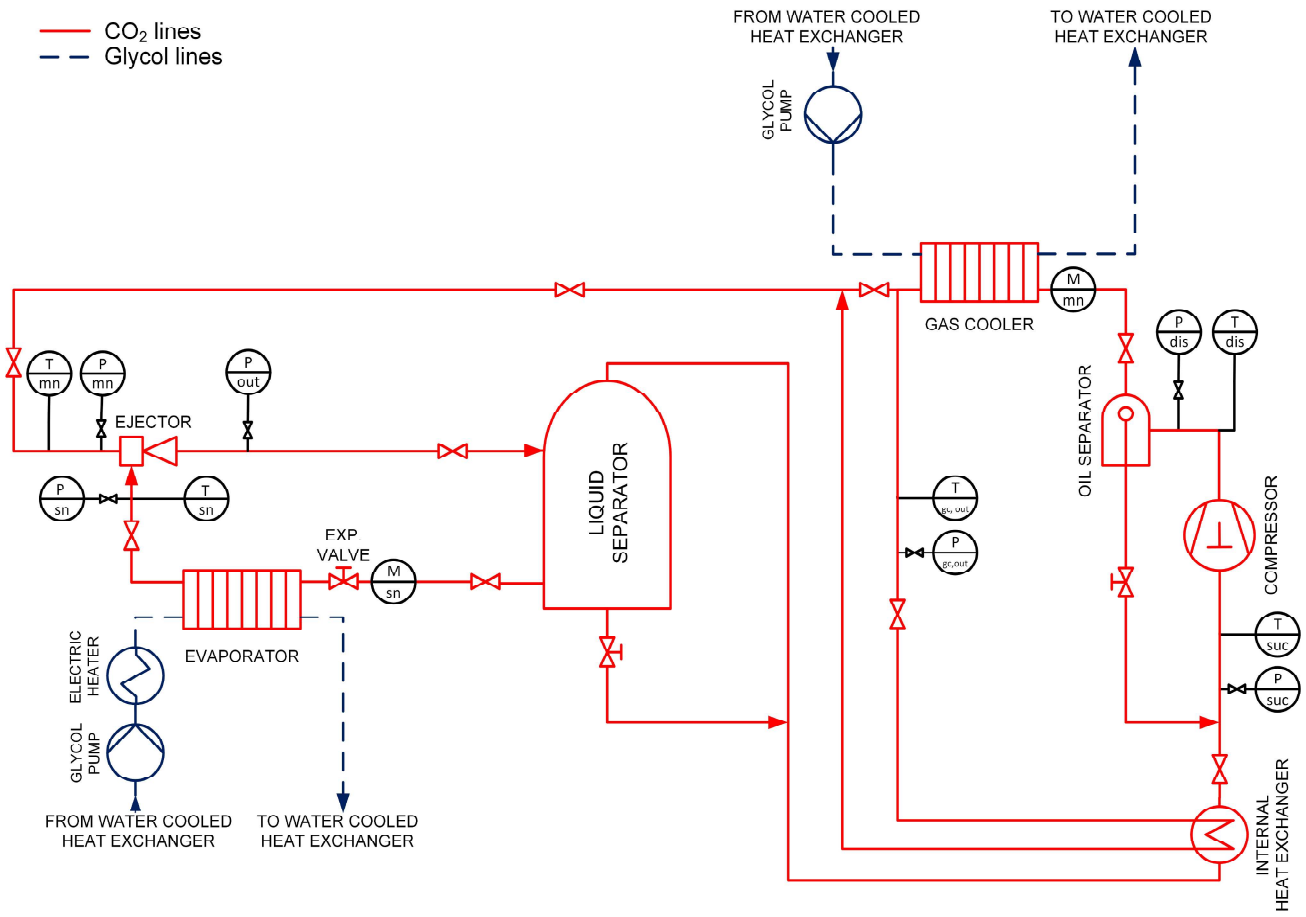

Figure 2: Scheme of the test rig with the CO_2 ejector as an expansion device.

multiple sight glasses to monitor the level of the liquid R744 inside. A 54% glycol-water solution with a freezing point of -42°C was used as a medium to absorb and reject the heat from the gas cooler and to the evaporator, respectively. Additionally, in the evaporator loop, the fluid flowed through an electric heater.

The glycol was cooled down in a glycol-water heat exchanger. Water was supplied using the main water installation and circulated between the test setup and a compensating reservoir. The water was cooled in a water-air heat exchanger. Fresh water could also be fed into the compensating reservoir.

The test rig also consisted of an advanced control system. The rotational speed of the compressor was adjusted by a transistor inverter in a range from 0 to 1450 rmp. Inverters also controlled the frequency of the glycol pumps. The electric heater was equipped with a terminal box with a thermostat to control the temperature of the glycol before entering the evaporator. A computer connected to the control cabinet allows an operator to activate and control the system using a National Instruments control unit via a LabView software panel.

This is the accepted version of an article published in Energy.
DOI: 10.1016/j.energy.2019.02.097

Table 1: Test facility equipment

Device	**Specification**
Ejector	prototype
Compressor	DORIN CD38OH
Compressor inverter	TOSHIBA VF-S7
Gas cooler	KAORI K040C-20C
Evaporator	KAORI K040C-12C
Liquid separator	prototype
Glycol pumps	GRUNDFOS CHI 2-50 A-W-G-BQQV
Glycol pumps inverters	TOSHIBA VF-S11
Electric heater	BACKER 10 kW

Measuring instruments

The multifunctional test setup contained calibrated measuring equipment, including Coriolis-type mass flow metres; piezoelectric absolute pressure and differential pressure sensors; T-type thermocouples; and resistive temperature sensors. All instruments were satisfactorily accurate and provided repeatable measurements. In Tab. 2, the specifications of each instrument are shown. Only equipment that was required to produce the key results of this study are included.

The x symbol used in Tab. 2 corresponded to the measured value. The range for the pressure sensors was defined in Eq. 1.

$$range = maximum\ of\ the\ set\ span - minimum\ of\ the\ set\ span \tag{1}$$

As shown in Tab. 2, two reference values were used for the T-type Thermocouples Cu-CuNi. The lower and higher accuracies corresponded to the positive and negative value of x, respectively.

The data read by the instruments were visible in real-time in the LabView software panel and were logged at a time interval of 10 s into a Microsoft Excel file.

2.2. Examined devices

Capillary tube

The capillary tube was a prototype expansion device manufactured at the NTNU/SINTEF laboratory in Trondheim. The tube is shown in Fig. 3, where its inlet and outlet parts are indicated. This simple expansion instrument was made of a stainless-steel pipe with an inlet diameter of 1.7 mm and an overall height of 160 mm. The tube was curved several times at a 90° angle. The horizontal projection of the tube was a rectangle that was 185 mm and 145 mm long. The tube was made of 6 similar sections with the same length and number of bends. The sections

This is the accepted version of an article published in Energy.
DOI: 10.1016/j.energy.2019.02.097

Table 2: Measuring instruments used in experiments

Measuring instrument	**Set span**	**Reference accuracy**
Absolute pressure transmitters		
Endress and Hauser Cerabar S PMP71	70 – 140 bar	$\pm 0.15\% \cdot range$
Endress and Hauser Cerabar S PMP71	40 – 140 bar	$\pm 0.15\% \cdot range$
Differential pressure transmitters		
Endress and Hauser Deltabar S PMD75	0 – 7 bar	$\pm 0.075\% \cdot range$
Endress and Hauser Deltabar S PMD75	0 – 10 bar	$\pm 0.075\% \cdot range$
Endress and Hauser Deltabar S PMD75	0 – 16 bar	$\pm 0.075\% \cdot range$
Mass flow meters		
Rheonic RHE08 RHM04	0.2 – 10 kg/min	$\pm 0.2\% \cdot x$
Rheonic RHE08 RHM06	0.5 – 20 kg/min	$\pm 0.2\% \cdot x$
Temperature measurement		
Thermocouples Cu-CuNi: Omega TMTSS	-200 – 350°C	$\pm 0.75\%$ or $1.5\% \cdot x$
Resistant RTD Sensors: Omega PT100	-30 – 300°C	$\pm 0.15 + 0.002 \cdot x$

were connected with Swagelok cross-type fittings to allow for pressure and temperature measurements between the sections. Four out of seven measuring points are also indicated in Fig. 3.

Prototype R744 ejector

The prototype CO_2 ejector was designed and manufactured by the *ejectorPL* group at the Silesian University of Technology, Gliwice, Poland. The ejector consisted of motive and suction nozzles, and mixer and diffuser parts. The motive nozzle was designed as a converging-diverging nozzle with a throat diameter of 1 mm to allow the CO_2 to expand after reaching the speed of sound in the motive nozzle throat. The ejector was connected to the test facility using the Swagelok system.

The prototype ejector was equipped with 13 drilled thermocouple channels to allow for wall temperature measurements near the inner surface of the ejector.

2.3. Measurements specification and settings

Capillary tube experiment

Omega RTD temperature sensors were placed at the inlet and outlet and between all the sections in direct contact with the refrigerant inside the tube (T_1 – T_7), as shown in Fig. 1. The absolute pressure was measured at three points: inlet (P_{IN}), outlet (P_{OUT}), and in the middle of the tube (P_{MID}). The pressure drop in each section was measured using differential pressure sensors (DP_{1-2} – DP_{6-7}). The mass flow of refrigerant was measured by Rheonic RHM06 mass flow metre (M).

This is the accepted version of an article published in Energy.
DOI: 10.1016/j.energy.2019.02.097

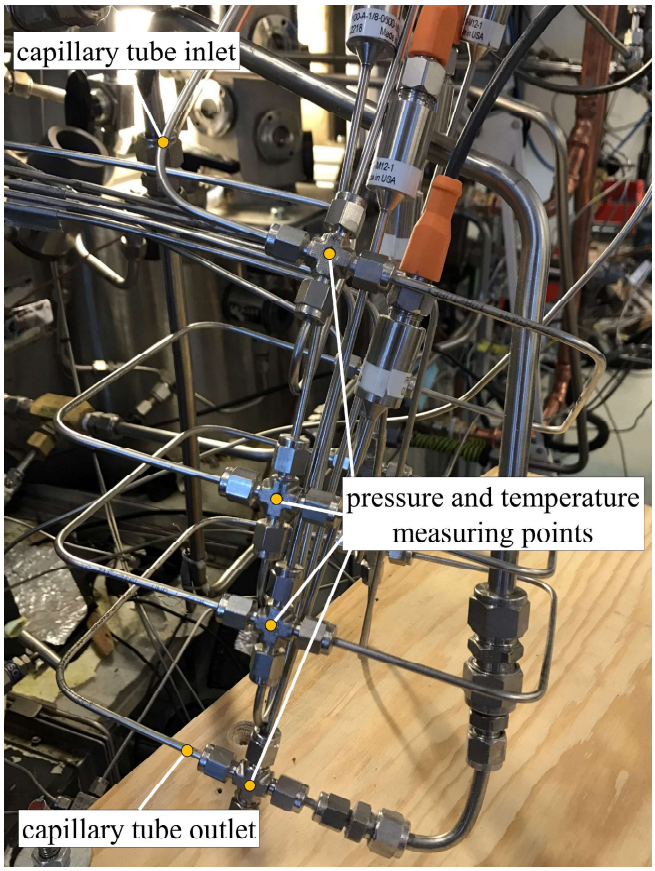

Figure 3: Capillary tube installed in the test rig.

Two test campaigns were performed. In the first campaign, the capillary tube was thermally insulated by placing it in a bucket filled with perlite, a material with a grained structure and a thermal conductivity of approximately 0.042 W/mK. Then, the capillary tube was fully buried in insulating material and the thickness of insulation was at least 2 cm. In the second campaign, the prototype expansion device was exposed to ambient conditions. The ambient temperature for all the measured locations ranged from 21.5°C to 23.7°C. The ambient temperature was relatively high and simulated realistic conditions of the machine-rooms of refrigeration system. The tests were performed at operating conditions typical for refrigeration systems. The absolute pressure of CO_2 at the inlet of capillary tube ranged from 64.5 bar to 92.2 bar, and the temperature ranged from 20.2°C to 31.3°C. The operating points investigated are described in Section 3.1. The inlet pressure and temperature were the key parameters and were controlled to obtain a wide variation of expansion curves. The CO_2 was kept as a supercritical fluid or a subcooled liquid at the inlet of the capillary tube.

Ejector experiment

In the test campaign with the ejector, the absolute pressure sensors were placed before the motive (P_{mn}) and suction (P_{sn}) nozzles, and after the outlet (P_{out}) of the ejector. Resistive sensors were used to measure the temperature at the motive (T_{mn}) and the suction nozzles (T_{sn}). The mass flow rate of the refrigerant was measured

This is the accepted version of an article published in Energy.
DOI: 10.1016/j.energy.2019.02.097

using Coriolis mass flow metres (Rheonic RHM04 and RHM06) at the motive (M_{mn}) and suction (M_{sn}) nozzles, respectively.

Temperature sensors were placed along the ejector axis, as shown in Fig. 4, where components of ejector are indicated. Thermocouples T_1 and T_2 measured the temperature at the wall of the motive nozzle inlet, while thermocouple T_3 measured the temperature between the motive and the suction nozzles. Temperatures $T_4 - T_8$ were measured at the suction nozzle wall. Finally, temperatures $T_9 - T_{13}$ were measured at the mixer and diffuser outer walls. The thermocouples placed in the drilled channels measured the wall temperatures 2 mm from the inner surface of the ejector. Thermal grease was applied at the bottom of each channel to provide better heat conduction between the thermocouple probes and the ejector wall.

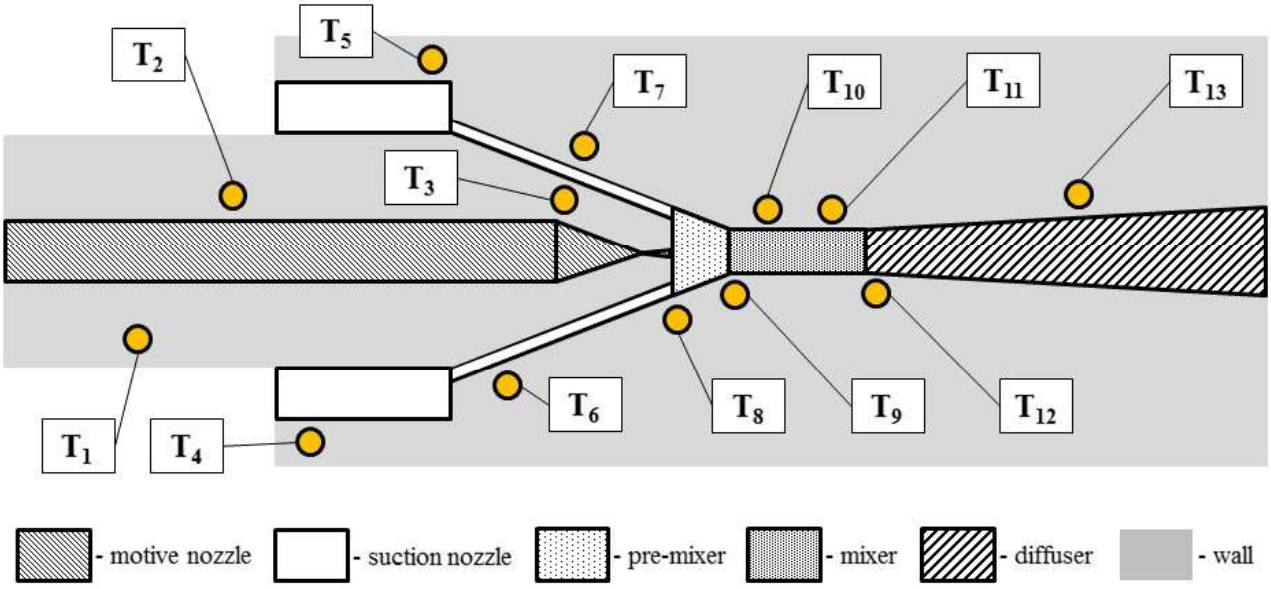

Figure 4: Schematic distribution of thermocouples probes along the prototype ejector.

The measurements collected for the prototype ejector simulated conditions typical for refrigeration systems. The absolute pressure of CO_2 at the motive inlet of ejector ranged from 71.3 bar to 106.3 bar, and the temperature ranged from 21.0°C to 33.8°C. The operating points investigated are described in Section 3.2. In most cases, supercritical conditions occurred at the motive inlet of the ejector. The tests were performed twice: once with a thermally insulated ejector, and once with a thermally uninsulated ejector. In the second part of this study, the ambient temperature was also measured. It ranged from 22.3°C to 25.3°C, what corresponded to conditions, which may occur in the machine-room of refrigeration system.

2.4. Data processing and uncertainty analyses

For all measurement locations, quasi steady-state conditions were obtained. System operation was considered to be at steady state when key parameters were constant or oscillating with a constant frequency. Measurements were then logged over a period of time between 6 and 10 minutes, which corresponded to 36 to 60 single readings.

This is the accepted version of an article published in Energy.
DOI: 10.1016/j.energy.2019.02.097

Then, the measured quantities were analysed. First, the average value of each measured quantity was calculated using Eq. 2, where x_i corresponds to single collected value, and n is the number of measurements.

$$\overline{x} = \frac{\sum_{i=1}^{n} x_i}{n} \tag{2}$$

The standard deviation was then used to calculate a random uncertainty (type A) using Eq. 3.

$$u_A = \sqrt{\frac{\sum_{i=1}^{n} (x_i - \overline{x})}{n(n-1)}} \tag{3}$$

The systematic uncertainty of the directly measured quantities (type B) was estimated using Eq. 4, where α is the reference accuracy of the measuring instrument, which was calculated for each device according to Tab. 2. A uniform (rectangular) probability distribution was assumed.

$$u_B = \frac{\alpha}{\sqrt{3}} \tag{4}$$

Finally, the combined standard deviation was calculated for each measured quantity using Eq. 5.

$$u = \sqrt{{u_A}^2 + {u_B}^2} \tag{5}$$

The thermodynamic properties of the CO2 were then calculated using REFPROP libraries [33]. The following characteristic parameters were then calculated, and the pressure lift of the ejector was calculated using Eq. 6.

$$P_{lift} = P_{out} - P_{sn} \tag{6}$$

The pressure ratio of the ejector was evaluated using Eq. 7.

$$P_{ratio} = \frac{P_{out}}{P_{sn}} \tag{7}$$

The mass entrainment ratio of the ejector was defined by Eq. 8.

$$\Phi_m = \frac{M_{sn}}{M_{mn}} \tag{8}$$

The ejector efficiency was determined using the definition reported in [34], which is the ratio between the recovered work of expansion to the maximal theoretical work recovery (Eq. 9).

$$\eta_{ej} = \Phi_m \frac{h(P_{out}, s_{sn}) - h_{sn}}{h_{mn} - h(P_{out}, s_{mn})} \tag{9}$$

In the numerator of Eq. 9, there is a difference between the specific enthalpy after isentropic compression of the suction fluid to the ejector outlet pressure ($h(P_{out}, s_{sn})$) and the enthalpy at the suction nozzle inlet (h_{sn}). In the denominator, there is a difference between the specific enthalpy at the motive nozzle inlet (h_{mn}) and the specific enthalpy after isentropic expansion of the motive fluid to the ejector outlet pressure ($h(P_{out}, s_{mn})$).

This is the accepted version of an article published in Energy.
DOI: 10.1016/j.energy.2019.02.097

Finally, the uncertainty of the calculated quantities was determined using the Law of Propagation of Uncertainty (Eq. 10), where the uncertainty of calculated quantity y was determined based on the uncertainty of the measured quantities x_i.

$$u(y) = \sqrt{\sum_{i=1}^{n} \left(\frac{\partial y}{\partial x_i} \right)^2 u^2(x_i)} \tag{10}$$

The partial derivatives of thermodynamic properties (e.g., the specific enthalpy, specific entropy) were computed from the derivative definition, as shown in Eq. 11, where the partial derivative of the specific enthalpy, which was calculated based on the absolute pressure and the specific entropy, was determined with respect to the specific entropy.

$$\left(\frac{\partial h}{\partial s} \right)_P = \lim_{\Delta s \to 0} \frac{h(P, s + \Delta s) - h(P, s)}{\Delta s} \tag{11}$$

Calculations were computed in Microsoft Excel using Visual Basic for Applications. Partial derivatives for the specific enthalpy evaluated at absolute pressure and temperature were estimated using the built-in REFPROP functions [33].

3. Results and discussion

3.1. Heat transfer influence in the capillary tube

In Fig. 5, the measured parameters obtained at the inlet of the capillary tube are shown for both cases: thermally insulated (adiabatic) and non-adiabatic walls. The characteristic operating conditions for the R744 refrigeration systems were examined. The inlet absolute pressure ranged from 64.5 bar to 92.2 bar, and the temperature ranged from 20.2°C to 31.3°C, corresponding to a few subcritical and a wide range of the supercritical operating points. The CO_2 was expanded in the capillary tube to pressures ranging from 34.3 bar to 46.7 bar. The average ambient temperature was of 22.6°C, when capillary tube without insulation was examined.

The maximum uncertainties were ±0.2 bar for the pressure measurements, ±0.2°C for the temperature measurements, ±0.1 kg/min for the mass flow rate measurements, and ±0.03 bar for the pressure difference measurements. The uncertainty of the calculated inlet specific enthalpy was ±1.6 kJ/kg.

In Fig. 6, the results for a few experimental conditions are shown. The absolute pressure, the temperature and the pressure difference between the beginning and the end of each section are shown for each point. The absolute pressure and temperature results are connected by a line to better visualize their variations. The pictures shown in the left column corresponded to the data collected for insulated capillary tube identified as capillary adiabatic (CA), while those in the right column corresponded to cases with non-adiabatic walls, or capillary non-adiabatic (CNA). In the second case, the temperature of the outer walls of the expansion device is also shown. The plots are arranged in pairs of similar inlet and outlet conditions to allow for easy comparison between the two experimental configurations.

Based on the results shown, the pressure is shown to decrease during expansion in the capillary tube. For each case, the pressure drop was relatively constant during expansion above the saturation line and increased suddenly

This is the accepted version of an article published in Energy.
DOI: 10.1016/j.energy.2019.02.097

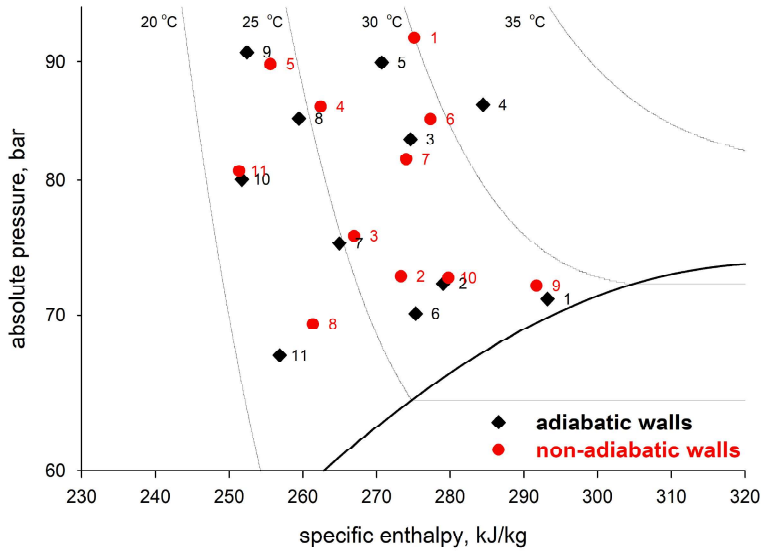

Figure 5: Experimental points at the inlet of insulated and uninsulated capillary tube.

into a two-phase region, which agrees with the literature [9, 13, 14, 17] for cases CA1 and CA8 and the corresponding cases CNA4 and CNA9. The CO_2 at the inlet of the expansion device at the operating point CA8 had supercritical parameters, while for case CA1, the inlet point was situated near above the saturation line, which is shown in the logp-h diagram of Fig. 5. Assuming isenthalpic expansion, R744 reached its saturation line when the pressure decreased to 58.7 bar and 69.8 bar for points CA8 and CA1, respectively. Thus, for point CA8, the pressure drop was nearly constant along the capillary tube, and the sudden pressure drop was visible only in the last two sections, where two-phase flow occurred. Conversely, the pressure drop for point CA1, which was near the saturation line, began to increase after the inlet of capillary tube.

For points CNA4, CNA11 and CNA9, the ambient temperature was of 22.5°C, 22.5°C and 21.5°C, respectively. For each point, the measured wall temperature seemed to be plausible based on the heat flux direction. This temperature was lower than the fluid temperature at CO_2 temperatures higher than the ambient temperature and higher than the fluid temperature at CO_2 temperatures lower than the ambient temperature. For the insulated capillary tube and the corresponding operating point after removing the thermal insulation, the influence of the ambient conditions was negligible during the experiment. The absolute pressure, pressure drop and temperature measurements were similar.

3.2. Heat transfer influence in prototype ejector

The experimental points collected for the prototype ejector are shown on the logp-h diagrams of Fig. 7. The parameters at the motive (on the left) and the suction (on the right) nozzle inlets were identified by indexes. A total of 15 points were examined for the ejector with thermal insulation, and 15 points were examined for the ejector with non-adiabatic walls. The pressure at the motive nozzle was maintained between 71.3 bar and 106.3 bar, while

This is the accepted version of an article published in Energy.
DOI: 10.1016/j.energy.2019.02.097

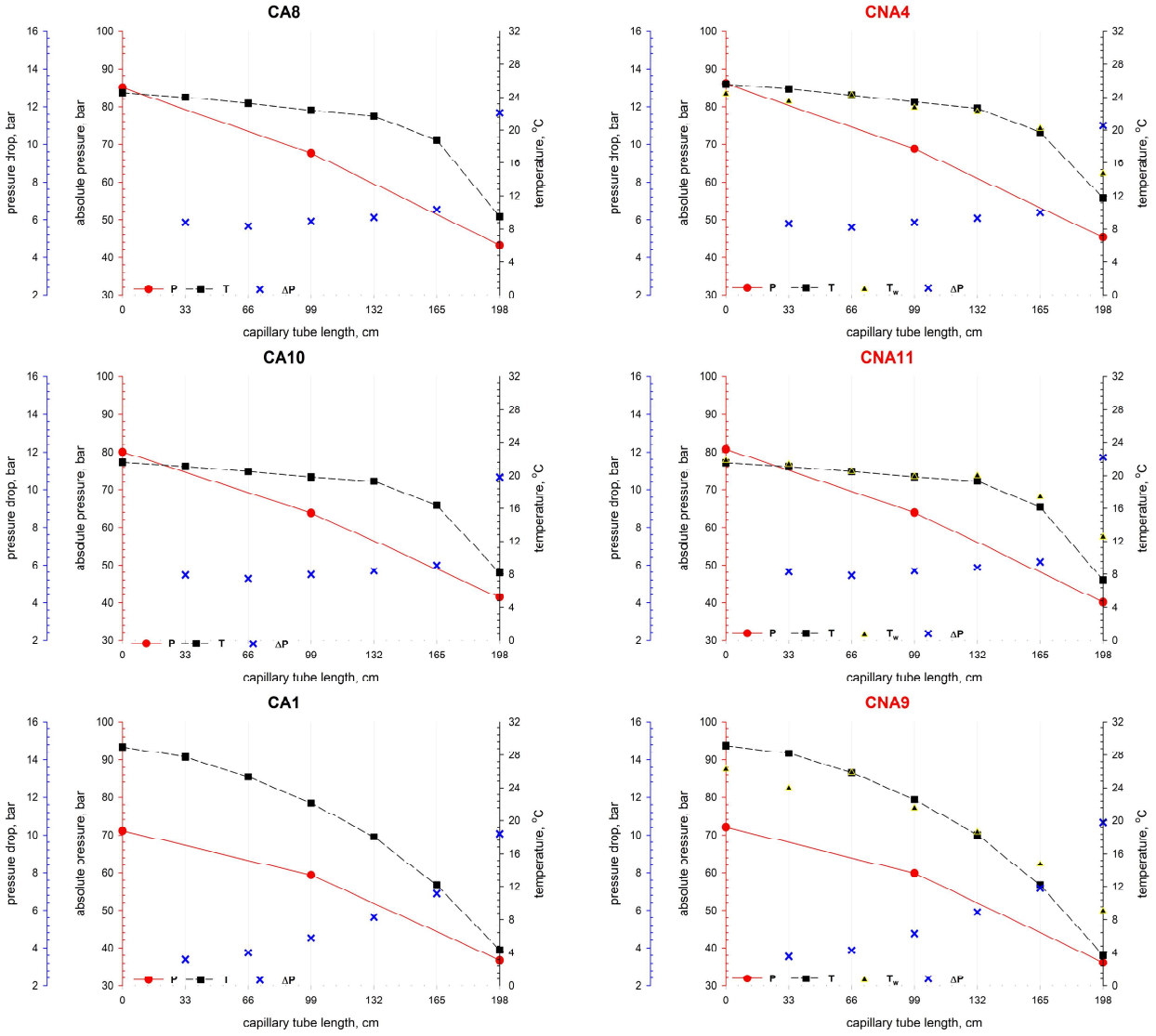

Figure 6: Absolute pressure, temperature and pressure difference for each section of the capillary tube with thermally insulated walls (left column) for operating points CA8, CA10 and CA1 and the corresponding cases CNA4, CNA11 and CNA9 without insulation (right column).

the temperature was maintained between 21.0°C and 33.8°C, corresponding to supercritical-gas or subcooled-liquid conditions. The operating conditions at the suction nozzle were related to those at the outlet of evaporator in the refrigeration system. The absolute pressure thus ranged from 24.2 bar to 33.8 bar. The suction stream was superheated from 4.9 K to 22.4 K, and the pressure of the two-phase fluid at the ejector outlet ranged from 25.9 bar to 41.7 bar. The ambient temperature was measured for ejector with non-adiabatic walls. The average value of this parameter was of 24.2°C. The maximum uncertainty of the absolute pressure was of ±0.09 bar for P_{mn} and ±0.03 bar for both P_{sn} and P_{out}. The highest uncertainty in the measured fluid temperatures at both inlets was ±0.13°C. The mass flow rate measurements ranged from 1.01 kg/min to 2.02 kg/min at the motive nozzle and from

This is the accepted version of an article published in Energy.
DOI: 10.1016/j.energy.2019.02.097

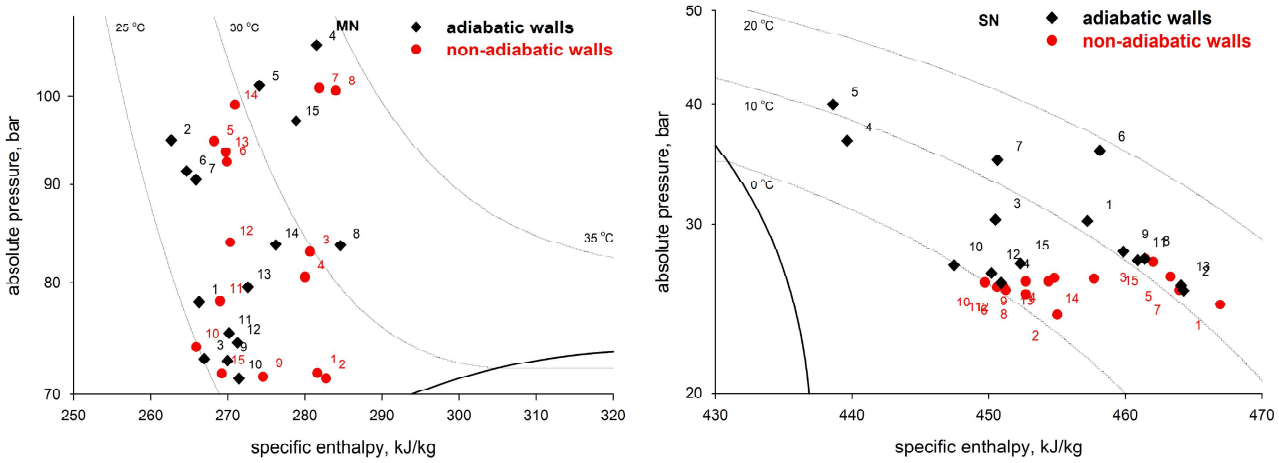

Figure 7: Experimental points at the motive (left) and suction (right) nozzle of the prototype ejector.

0.38 kg/min to 1.15 kg/min at the suction nozzle with a maximal standard deviation of ±0.03 kg/min.

In Tab. 3, six experimental points for the ejector with thermal insulation (ejector adiabatic, or EA) are compared with comparable points for the ejector without insulation (ejector non-adiabatic, or ENA). However, the thermodynamic parameters were not equal in each pair of cases due to difficulties with obtaining the same working conditions in the test setup.

As shown the table, a wide range of parameters at the motive nozzle inlet of the ejector were selected. Most results coincided with supercritical conditions except the last point in both sections of the table. The absolute pressure at the suction nozzle was similar for all the cases presented in Tab. 3 and ranged from 25.8 bar to 27.3 bar. The ambient temperature for ejector with non-adiabatic walls ranged from 24.0°C for ENA9 to 25.2°C for ENA14, providing significant temperature difference in regard to the suction stream. It allowed an assessment of the heat transfer influence on ejector operation. The pressure ratio determined for both series of measurements ranged from 1.05 to 1.09 with an uncertainty of ±0.001. The maximal mass entrainment ratio was 0.48 for cases ENA14 and ENA10. The highest ejector efficiency was 0.16 for point EA2. The maximum uncertainty of the mass entrainment ratio was ±0.03; however, in most cases, it was below ±0.01. For the ejector efficiency, uncertainty was high compared to the estimated results because its value depends on five calculated quantities. For example, as shown in Tab. 3, this uncertainty ranged from ±0.01 for point EA8 to ±0.03 for point EA10. The ranges of the standard deviation corresponded to between 29% and 59% of the estimated ejector efficiency.

Based on the results shown in Tab. 3, thermal insulation did not have a significant effect on ejector efficiency. Exceptions are noted for two pairs of operating points (EA15 and ENA14, EA2 and ENA5), where ejector efficiency decreased by 4 and 5 percentage points with the non-adiabatic ejector, respectively. However, for cases EA15 and ENA14, the pressure and temperature at the motive nozzle inlet varied between 2% and 6%, respectively. Small changes in those parameters were thus important at high pressures and temperatures. Additionally, the pressure ratio differed in both cases; thus, it was difficult to describe how the thermal insulation affected the system. For

This is the accepted version of an article published in Energy.
DOI: 10.1016/j.energy.2019.02.097

Table 3: Comparable operating points and characteristic parameters for thermally insulated and uninsulated prototype ejector

No.	P_{mn}	T_{mn}	P_{sn}	T_{sn}	P_{out}	M_{mn}	M_{sn}	T_{amb}	P_{ratio}	ΔT	Φ_m	η_{ej}
–	bar	°C	bar	°C	bar	kg/min	kg/min	°C	–	K	–	–
Thermally insulated ejector												
EA15	97.1	31.7	27.3	3.6	29.8	1.7	0.8		1.09	28.1	0.46	0.12
EA2	94.9	26.6	25.6	11.1	27.4	1.6	1.0		1.07	15.5	0.64	0.16
EA8	83.6	30.9	27.6	11.3	29.6	1.3	0.5		1.07	19.6	0.36	0.09
EA14	83.7	29.0	26.1	0.8	28.2	1.4	0.6		1.08	28.2	0.44	0.12
EA12	74.5	26.3	26.7	1.1	28.2	1.3	0.6		1.06	25.2	0.45	0.10
EA10	71.3	25.8	27.2	-0.2	28.5	1.2	0.5		1.05	26.0	0.47	0.09
Thermally uninsulated ejector												
ENA14	99.0	29.7	26.3	6.6	27.8	1.9	0.9	25.2	1.06	23.0	0.48	0.08
ENA5	94.8	28.3	26.5	11.4	28.3	1.8	0.8	24.3	1.07	16.9	0.45	0.11
ENA3	83.0	29.9	27.6	11.3	29.6	1.3	0.6	24.2	1.07	18.6	0.44	0.12
ENA12	83.9	27.5	25.8	0.6	27.6	1.5	0.7	24.6	1.07	26.9	0.46	0.11
ENA10	74.1	24.9	26.1	-0.1	27.4	1.3	0.6	24.2	1.05	25.0	0.48	0.10
ENA9	71.5	26.4	26.1	2.4	27.6	1.1	0.5	24.0	1.06	24.1	0.43	0.09

points EA2 and ENA5, the conditions at the motive nozzle inlet were intended to be sufficiently similar to compare both cases; however, the mass entrainment ratio and thus the ejector efficiency decreased by approximately 30%. This change could be caused by unstable work in the compressor due to high-pressure ratios between the suction and discharge connectors. Measurements for these two points should be repeated. For all remaining points, the ejector efficiency was similar in both configurations, and any differences fell within the range of computed uncertainties.

The effects of the insulation on the ejector wall temperature were also investigated. The results for points EA10 and EA8 are compared to those at points ENA9 and ENA3 in Fig. 8. Thermocouples $1 - 13$ are related to the indexes shown in Fig. 4.

The highest temperature differences between the insulated and uninsulated ejectors occurred at the motive nozzle. However, in this part of ejector, the temperature was strongly affected by the heat transfer between the motive and suction fluids; thus, the effects of the thermal insulation were difficult to determine. For the last 10 temperatures measured near the suction nozzle, mixer and diffuser walls, the wall temperature was higher by 0.1 K to 1.2 K in all cases for the uninsulated ejector. For temperatures T_{10}, T_{11} and T_{13} for points EA8 and ENA3, this difference was between 0.7 K and 0.9 K. Those measurements were particularly important because of their strong agreement in outlet pressures (0.2% difference) between the adiabatic and non-adiabatic configuration. These conditions resulted in similar thermal parameters of the CO_2 inside the diffuser. For temperature T_{12}, the

This is the accepted version of an article published in Energy.
DOI: 10.1016/j.energy.2019.02.097

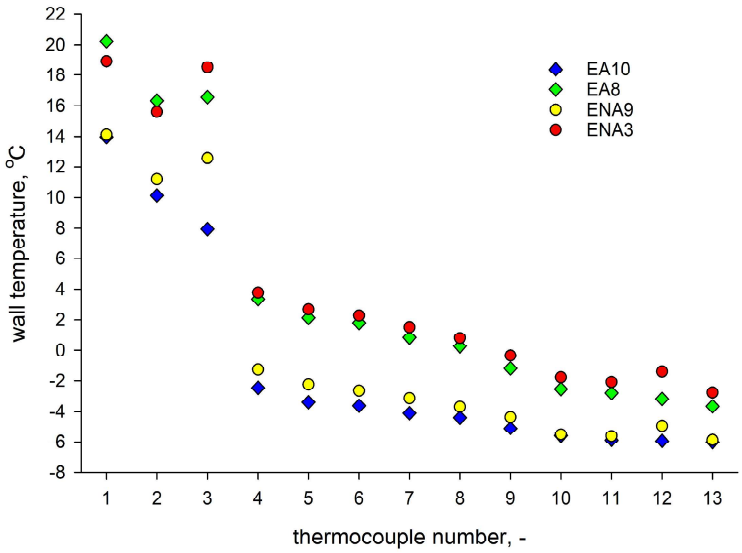

Figure 8: Wall temperature comparison between thermally insulated and uninsulated ejector.

difference was more significant and likely indicated a problem with the measurement instrument.

Based on the above considerations, the ejectors thermal insulation was found to have a small effect on the thermal parameters inside the ejector.

In Tab. 4, two pairs of experimental points are compared and are shown to vary by temperature difference at the motive and the suction nozzle inlets. However, the parameters of R744 at the motive nozzle inlet were maintained at the same level. The ambient temperature was kept at similar level for points ENA1 and ENA2 and differed by 1.1 K for points ENA7 and ENA8. All the results presented in that table were determined for the ejector without thermal insulation. Decreasing the temperature at the outlet of evaporator only slightly affected the suction nozzle and outlet pressure. This temperature difference thus did not significantly affect ejector performance. The mass entrainment ratio changed only due to the density increase caused by the decrease in temperature.

Table 4: Comparable operating points and characteristic parameters for various temperature difference between R744 at the motive and suction nozzle inlets.

No.	P_{mn}	T_{mn}	P_{sn}	T_{sn}	P_{out}	M_{mn}	M_{sn}	T_{amb}	P_{ratio}	ΔT	Φ_m	η_{ej}
–	bar	°C	bar	°C	bar	kg/min	kg/min	°C	–	K	–	–
ENA1	71.8	27.8	24.8	12.4	26.5	1.0	0.4	23.9	1.07	15.4	0.37	0.09
ENA2	71.3	27.8	24.2	1.5	25.9	1.0	0.4	23.6	1.07	26.4	0.39	0.09
ENA7	101.0	33.1	25.6	10.9	28.4	1.8	0.7	24.0	1.11	22.2	0.41	0.13
ENA8	100.7	33.7	25.4	1.3	28.3	1.7	0.7	25.1	1.11	32.4	0.42	0.13

This is the accepted version of an article published in Energy.
DOI: 10.1016/j.energy.2019.02.097

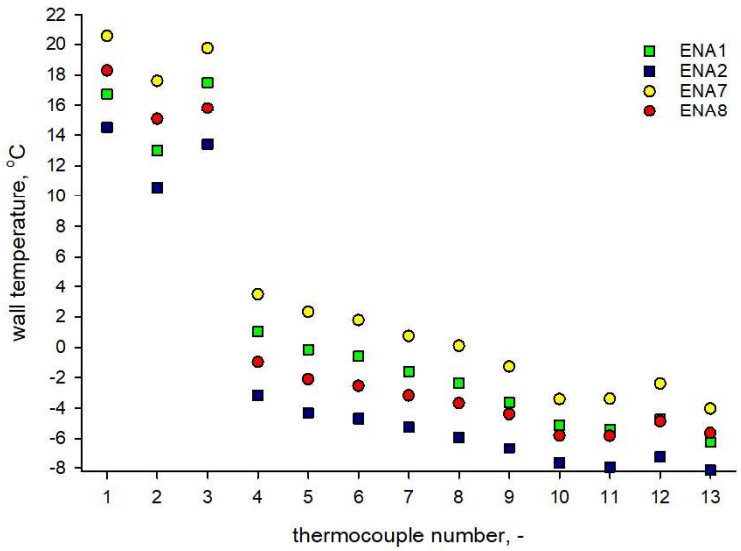

Figure 9: Wall temperature comparison between experimental points with different ΔT parameter.

The influence of the temperature difference between the motive and suction nozzle fluids on the wall temperatures of the ejector was also examined and are shown in Fig. 9 for all four points from the above table. The wall temperature for the points with lower suction fluid temperatures (ENA2 and ENA8) decreased at most to the points that correspond to ENA1 and ENA7, respectively. The difference between wall temperatures for points ENA1 and ENA2 was between 1.9 K and 4.2 K and those for points ENA7 and ENA8 was between 1.6 K and 4.5 K. Thus, the suction nozzle temperature affected the temperatures across the ejector and thus also the temperature of the motive nozzle part. The temperature values recorded at sensor location 3 were between the motive and suction fluid temperatures, indicating that heat transfer occurred between those fluid streams. The wall temperature difference was the highest for thermocouple 4 but decreased on both sides along the ejector.

The insulation of the ejector does not significantly impact ejector performance. Thus, considering the ejectors external walls to be non-adiabatic or adiabatic will not affect numerical investigations of an R744 two-phase flow through an ejector. This result contradicts the conclusions of Milazzo et al. [31], who investigated ejector operation with a different refrigerant.

4. Conclusions

In this study, experimental tests were performed at the SINTEF/NTNU laboratory in Trondheim, Norway using a capillary tube and a prototype ejector as expansion devices in a R744 transcritical refrigeration system. The effects of heat transfer between the capillary tube or ejector wall and the ambient environment on the performance of these expansion devices were examined. For both the capillary tube and ejector, operating conditions that are typical for R744 refrigeration systems were selected. The ambient temperature corresponded to realistic conditions, that

This is the accepted version of an article published in Energy.
DOI: 10.1016/j.energy.2019.02.097

occur in the machine-room of the refrigeration system.

The examination of the capillary tube provided plausible results regarding the temperature and pressure profiles of the refrigerant along the expansion device. The pressure and temperature drop were found to be higher when supercritical CO_2 reached the saturation line during expansion in the capillary tube. Ambient conditions were not found affect the CO_2 flow inside the tube.

The examination of the prototype ejector, which was designed to measure the temperature of the wall near the inner surface, included an investigation of a wide range of operating conditions. Thermal insulation did not significantly affect ejector efficiency or the temperature of the ejector wall. Thus, selecting a non-adiabatic or adiabatic boundary condition for a R744 ejector wall in a numerical study should not affect results in a CO_2 two-phase flow analysis. The difference between the suction and motive fluid temperature also showed negligible effects on ejector performance.

Acknowledgement

The authors gratefully acknowledge the financial support of the Research Council of Norway through project No. 244009/E20. This paper has been also co-funded by HighEFF - Centre for an Energy Efficient and Competitive Industry for the Future, an 8-year Research Centre under the FME-scheme (Centre for Environment-friendly Energy Research, 257632/E20). The authors gratefully acknowledge the financial support from the Research Council of Norway and user partners of HighEFF. The work of MH was also partially supported by the Rectors research grant No. 08/060/RGJ18/0157 provided by SUT.

References

[1] United Nations Environment Programme (UNEP), Montreal Protocol on substances that deplete the ozone layer (1987).

[2] United Nations Framework Convention On Climate Change (UNFCCC), Kyoto Protocol (1997).

[3] The European Parliament and the European Council, Regulation (EU) No 517/2014 of the European Parliament and of the Council of 16 April 2014 on fluorinated greenhouse gases and repealing Regulation (EC) No 842/2006 (1), OJ 57 (L 150) (2014) 195–230.

[4] N. Abas, A. R. Kalair, N. Khan, A. Haider, Z. Saleem, M. S. Saleem, Natural and synthetic refrigerants, global warming: A review, Renewable and Sustainable Energy Reviews 90 (2018) 557 – 569. doi:https://doi.org/10.1016/j.rser.2018.03.099.
URL http://www.sciencedirect.com/science/article/pii/S1364032118301977

[5] G. Lorentzen, Revival of carbon dioxide as a refrigerant, International Journal of Refrigeration 17 (5) (1994) 292 – 301. doi:https://doi.org/10.1016/0140-7007(94)90059-0.
URL http://www.sciencedirect.com/science/article/pii/0140700794900590

[6] N. Agrawal, S. Bhattacharyya, Experimental investigations on adiabatic capillary tube in a transcritical co2 heat pump system for simultaneous water cooling and heating, International Journal of Refrigeration 34 (2) (2011) 476 – 483. doi:https://doi.org/10.1016/j.ijrefrig.2010.09.014.
URL http://www.sciencedirect.com/science/article/pii/S0140700710002227

This is the accepted version of an article published in Energy.
DOI: 10.1016/j.energy.2019.02.097

[7] N. Agrawal, S. Bhattacharyya, Adiabatic capillary tube flow of carbon dioxide in a transcritical heat pump cycle, International Journal of Energy Research 31 (11) 1016–1030. arXiv:https://onlinelibrary.wiley.com/doi/pdf/10.1002/er.1294, doi:10.1002/er.1294.
URL https://onlinelibrary.wiley.com/doi/abs/10.1002/er.1294

[8] K. B. Madsen, C. S. Poulsen, M. Wiesenfarth, Study of capillary tubes in a transcritical co2 refrigeration system, International Journal of Refrigeration 28 (8) (2005) 1212 – 1218, cO2 as Working Fluid - Theory and Applications. doi:https://doi.org/10.1016/j.ijrefrig.2005.09.009.
URL http://www.sciencedirect.com/science/article/pii/S0140700705001726

[9] D. L. da Silva, C. J. Hermes, C. Melo, J. M. Gonalves, G. C. Weber, A study of transcritical carbon dioxide flow through adiabatic capillary tubes, International Journal of Refrigeration 32 (5) (2009) 978 – 987. doi:https://doi.org/10.1016/j.ijrefrig.2008.10.010.
URL http://www.sciencedirect.com/science/article/pii/S014070070800203X

[10] Y. Song, J. Wang, F. Cao, P. Shu, X. Wang, Experimental investigation on a capillary tube based transcritical co2 heat pump system, Applied Thermal Engineering 112 (2017) 184 – 189. doi:https://doi.org/10.1016/j.applthermaleng.2016.10.033.
URL http://www.sciencedirect.com/science/article/pii/S1359431116322396

[11] Y. Song, J. Wang, F. Cao, P. Shu, X. Wang, Investigation on the adaptivity of the transcritical co2 refrigeration system with a capillary, International Journal of Refrigeration 79 (2017) 183 – 195. doi:https://doi.org/10.1016/j.ijrefrig.2017.04.013.
URL http://www.sciencedirect.com/science/article/pii/S0140700717301494

[12] D. Wang, Y. Lu, L. Tao, Optimal combination of capillary tube geometry and refrigerant charge on a small co2 water-source heat pump water heater, International Journal of Refrigeration 88 (2018) 626 – 636. doi:https://doi.org/10.1016/j.ijrefrig.2018.03.009.
URL http://www.sciencedirect.com/science/article/pii/S0140700718300884

[13] D. L. da Silva, A. F. Ronzoni, C. Melo, C. J. Hermes, A study of transcritical carbon dioxide flow through diabatic capillary tubes, International Journal of Refrigeration 34 (4) (2011) 834 – 843. doi:https://doi.org/10.1016/j.ijrefrig.2011.02.010.
URL http://www.sciencedirect.com/science/article/pii/S0140700711000569

[14] N. Agrawal, S. Bhattacharyya, Homogeneous versus separated two phase flow models: Adiabatic capillary tube flow in a transcritical co2 heat pump, International Journal of Thermal Sciences 47 (11) (2008) 1555 – 1562. doi:https://doi.org/10.1016/j.ijthermalsci.2007.12.008.
URL http://www.sciencedirect.com/science/article/pii/S1290072907002700

[15] N. Agrawal, S. Bhattacharyya, Optimized transcritical co2 heat pumps: Performance comparison of capillary tubes against expansion valves, International Journal of Refrigeration 31 (3) (2008) 388 – 395. doi:https://doi.org/10.1016/j.ijrefrig.2007.08.006.
URL http://www.sciencedirect.com/science/article/pii/S014070070700165X

[16] C. J. Hermes, D. L. da Silva, C. Melo, J. M. Gonalves, G. C. Weber, Algebraic solution of transcritical carbon dioxide flow through adiabatic capillary tubes, International Journal of Refrigeration 32 (5) (2009) 973 – 977. doi:https://doi.org/10.1016/j.ijrefrig.2008.10.006.
URL http://www.sciencedirect.com/science/article/pii/S0140700708002053

[17] N. Agrawal, S. Bhattacharyya, Non-adiabatic capillary tube flow of carbon dioxide in a transcritical heat pump cycle, Energy Conversion and Management 48 (9) (2007) 2491 – 2501. doi:https://doi.org/10.1016/j.enconman.2007.04.012.
URL http://www.sciencedirect.com/science/article/pii/S0196890407001069

This is the accepted version of an article published in Energy.
DOI: 10.1016/j.energy.2019.02.097

[18] P. Gullo, B. Elmegaard, G. Cortella, Advanced exergy analysis of a r744 booster refrigeration system with parallel compression, Energy 107 (2016) 562 – 571. doi:https://doi.org/10.1016/j.energy.2016.04.043.
URL http://www.sciencedirect.com/science/article/pii/S0360544216304492

[19] J. Sarkar, Optimization of ejector-expansion transcritical co2 heat pump cycle, Energy 33 (9) (2008) 1399 – 1406. doi:https://doi.org/10.1016/j.energy.2008.04.007.
URL http://www.sciencedirect.com/science/article/pii/S0360544208000984

[20] J. S. Lee, M. S. Kim, M. S. Kim, Experimental study on the improvement of co2 air conditioning system performance using an ejector, International Journal of Refrigeration 34 (7) (2011) 1614 – 1625, ejector Technology. doi:https://doi.org/10.1016/j.ijrefrig.2010.07.025.
URL http://www.sciencedirect.com/science/article/pii/S0140700710001714

[21] C. Lucas, J. Koehler, Experimental investigation of the cop improvement of a refrigeration cycle by use of an ejector, International Journal of Refrigeration 35 (6) (2012) 1595 – 1603. doi:https://doi.org/10.1016/j.ijrefrig.2012.05.010.
URL http://www.sciencedirect.com/science/article/pii/S0140700712001247

[22] K. Banasiak, A. Hafner, T. Andresen, Experimental and numerical investigation of the influence of the two-phase ejector geometry on the performance of the r744 heat pump, International Journal of Refrigeration 35 (6) (2012) 1617 – 1625. doi:https://doi.org/10.1016/j.ijrefrig.2012.04.012.
URL http://www.sciencedirect.com/science/article/pii/S014070071200093X

[23] S. Minetto, R. Brignoli, K. Banasiak, A. Hafner, C. Zilio, Performance assessment of an off-the-shelf r744 heat pump equipped with an ejector, Applied Thermal Engineering 59 (1) (2013) 568 – 575. doi:https://doi.org/10.1016/j.applthermaleng.2013.06.032.
URL http://www.sciencedirect.com/science/article/pii/S1359431113004572

[24] J. S. Lee, M. S. Kim, M. S. Kim, Studies on the performance of a co2 air conditioning system using an ejector as an expansion device, International Journal of Refrigeration 38 (2014) 140 – 152. doi:https://doi.org/10.1016/j.ijrefrig.2013.08.019.
URL http://www.sciencedirect.com/science/article/pii/S0140700713002272

[25] M. Palacz, J. Smolka, W. Kus, A. Fic, Z. Bulinski, A. J. Nowak, K. Banasiak, A. Hafner, Cfd-based shape optimisation of a co2 two-phase ejector mixing section, Applied Thermal Engineering 95 (2016) 62 – 69. doi:https://doi.org/10.1016/j.applthermaleng.2015.11.012.
URL http://www.sciencedirect.com/science/article/pii/S1359431115012478

[26] M. Nakagawa, A. Marasigan, T. Matsukawa, A. Kurashina, Experimental investigation on the effect of mixing length on the performance of two-phase ejector for co2 refrigeration cycle with and without heat exchanger, International Journal of Refrigeration 34 (7) (2011) 1604 – 1613, ejector Technology. doi:https://doi.org/10.1016/j.ijrefrig.2010.07.021.
URL http://www.sciencedirect.com/science/article/pii/S0140700710001672

[27] F. Liu, E. A. Groll, D. Li, Investigation on performance of variable geometry ejectors for co2 refrigeration cycles, Energy 45 (1) (2012) 829 – 839, the 24th International Conference on Efficiency, Cost, Optimization, Simulation and Environmental Impact of Energy, ECOS 2011. doi:https://doi.org/10.1016/j.energy.2012.07.008.
URL http://www.sciencedirect.com/science/article/pii/S0360544212005385

[28] L. Zheng, J. Deng, Research on co2 ejector component efficiencies by experiment measurement and distributed-parameter modeling, Energy Conversion and Management 142 (2017) 244 – 256. doi:https://doi.org/10.1016/j.enconman.2017.03.017.
URL http://www.sciencedirect.com/science/article/pii/S0196890417302200

[29] J. Bodys, J. Smolka, M. Palacz, M. Haida, K. Banasiak, A. J. Nowak, A. Hafner, Performance of fixed geometry ejectors with a swirl motion installed in a multi-ejector module of a co2 refrigeration system, Energy 117 (2016) 620 – 631, the 28th International

This is the accepted version of an article published in Energy.
DOI: 10.1016/j.energy.2019.02.097

Conference on Efficiency, Cost, Optimization, Simulation and Environmental Impact of Energy Systems - ECOS 2015. doi:https://doi.org/10.1016/j.energy.2016.07.037.
URL http://www.sciencedirect.com/science/article/pii/S0360544216309616

[30] M. Haida, J. Smolka, A. Hafner, Z. Ostrowski, M. Palacz, K. B. Madsen, S. Frsterling, A. J. Nowak, K. Banasiak, Performance mapping of the r744 ejectors for refrigeration and air conditioning supermarket application: A hybrid reduced-order model, Energy 153 (2018) 933 – 948. doi:https://doi.org/10.1016/j.energy.2018.04.088.
URL http://www.sciencedirect.com/science/article/pii/S0360544218306959

[31] A. Milazzo, F. Mazzelli, Future perspectives in ejector refrigeration, Applied Thermal Engineering 121 (2017) 344 – 350. doi:https://doi.org/10.1016/j.applthermaleng.2017.04.088.
URL http://www.sciencedirect.com/science/article/pii/S135943111732656X

[32] M. Haida, J. Smolka, A. Hafner, M. Mastrowski, M. Palacz, K. B. Madsen, A. J. Nowak, K. Banasiak, Numerical investigation of heat transfer in a co2 two-phase ejector, Energy 163 (2018) 682 – 698. doi:https://doi.org/10.1016/j.energy.2018.08.175.
URL http://www.sciencedirect.com/science/article/pii/S0360544218317110

[33] E. W. Lemmon, M. L. Huber, M. O. McLinden, NIST Standard Reference Database 23: Reference Fluid Thermodynamic and Transport Properties - REFPROP, Version 9.1, Standard Reference Data Program, National Institute of Standards and Technology, 2013.

[34] S. Elbel, P. Hrnjak, Experimental validation of a prototype ejector designed to reduce throttling losses encountered in transcritical r744 system operation, International Journal of Refrigeration 31 (3) (2008) 411 – 422. doi:https://doi.org/10.1016/j.ijrefrig.2007.07.013.
URL http://www.sciencedirect.com/science/article/pii/S0140700707001508

This is the accepted version of an article published in Energy.
DOI: 10.1016/j.energy.2019.02.097